Desalination and Water Treatment
www.deswater.com
doi: 10.5004/dwt.2023.30093

314 (2023) 231–240
December

Removal of Brilliant Green dye in aqueous solution using synthetic coagulation and flocculation technique

Senthil Kumar Muniasamy[a], Abeer A. AlObaid[b], Ismail Warad[c,d], Gokulan Ravindiran[e,*]

[a]*Department of Biotechnology, Karpaga Vinayaga College of Engineering and Technology, Kanchipuram-603 308, Tamil Nadu, India, email: senthilenvtce@gmail.com*
[b]*Department of Chemistry, College of Science, King Saud University, P.O. Box: 2455, Riyadh 11451, Saudi Arabia, email: aaalobaid@ksu.edu.sa*
[c]*Department of Chemistry, AN-Najah National University, P.O. Box: 7, Nablus, Palestine, email: i.kh.warad@gmail.com*
[d]*Research Centre, Manchester Salt & Catalysis, Unit C, 88-90 Chorlton Rd, M154AN Manchester, United Kingdom*
[e]*Department of Civil Engineering, VNR Vignana Jyothi Institute of Engineering and Technology, Hyderabad 500090, Telangana, India, email: gokulravi4455@gmail.com*

Received 17 June 2023; Accepted 28 October 2023

ABSTRACT

Brilliant green, also known as ethanaminium, is a triarylmethane dye derivative that has been employed as a coloring agent in the textile industry. A sizable volume of vivid green dye was made in a lab while the physio-chemical properties were investigated. This study looked at how to extract the brilliant green dye from the aqueous reagent using the coagulation–flocculation method to provide the desired features. Used as a flocculant and coagulant, respectively, polyaluminum chloride (PAC). Sodium bisulfate ($NaHSO_4$) solution and hydrochloric acid (HCl) employed to alter the pH during the treatment process. Different pH values and coagulant and flocculant dosages used in a series of jar tests. The supernatant aqueous effluent determined by numerous experimental studies termed turbidity, chemical oxygen demand (COD), colour, and suspended solids (SS) after every experimental analysis and after the practical investigation. The effectiveness of the treatment ranged from a turbidity reduction of 40%–98% to the elimination of 15%–99.2% of COD and a range of 20%–97.3% of suspended particles. In order to optimize removal efficiency, the optimal parameters for the entire quadratic model found using the analysis of variance (ANOVA). By using SEM, XRD, and FTIR analyses, the surface morphology of the sludge characterized. The treatment of brilliant green dye in aqueous solution identified as the successful solution by this coagulation–flocculation procedure using jar test equipment.

Keywords: Brilliant green; Coagulation; Flocculation; Synthetic coagulant; Surface characterization

1. Introduction

In numerous industries, including those that process food, make cosmetics, textiles, plastics, and paper, dyes are utilized extensively. A tenth of all dye products released into the waste stream during the production process [1]. Most of these colours escape traditional wastewater-treatment facilities, persist in the environment, and contaminate waterways. When this water is reprocessed by local humans, animals, and plants, it often becomes tainted with lethal toxins [2]. These are products made from synthetic dyes. It is made of dangerous chemical composites that are toxic to consume. The dye pollution is overrun and dye-contented, according to the two main issues [3]. Chemical mixtures

* Corresponding author.

that are toxic to living things are used to create synthetic colours. These businesses produce colours using low-cost ingredients and collect fees locally and internationally [4]. Brilliant green is a biological hydrogen sulphate salt with a counterion made up of four diethylamino phenyls. Its main character is a fluorochrome, an antibacterial medicine, a sterile agent, a venomous substance, and an environmental contaminant [5]. The network structure created by the molecular bars of the component parts of coagulant promotes coagulation–flocculation and bridge performance of coagulant as a flocculent compared with other experiment like adsorption, microfiltration and nano filtration. The findings of the pore size measurement are shown in the histogram. The histogram shows a hierarchy of pore types, from micropore to mesopore to fracture macropores [6]. The lowest and highest average crystalline sizes are also shown below the histogram [7]. The best methods for eliminating suspended particles and inorganic materials are coagulation and flocculation [8]. When present in high concentrations, many of these pollutants can make water taste bad and turn it brown or orange. The removal of suspended particles and harmful elements from the samples accomplished using coagulant [9]. They include molecules that are positively charged, which contributes to the efficient neutralization of water. Jar Test allows for the precise, ideal dosing of chemical coagulants intended to remove suspended particles and contaminants [10]. The best dosage and use of chemical coagulants are determined by the laboratory Jar test findings, which caricaturists a full-scale operation in the treatment process. Precipitation is the chemical process by which detectable constituents become discernible elements [11]. Coagulation and flocculation are based on a chemical reaction that promotes the development, aggregation, or clopping of such materials in order to allow for their exclusion from solution [12]. The dosage or quantity of a precipitant, coagulant, or flocculant needed to coagulate and remove the particles present in effluent relies on the concentration of the solution as well as a number of other factors, such as pH and chemical conditions [13]. This research explored coagulation and flocculation techniques were utilized in the current work to remove vivid green dye from wastewater. A jar test apparatus designed for laboratories is used for this. The focus of the investigation is on controlling factors such turbidity, COD, color, and suspended solids [14]. The regulation of the ideal pH and dosage for coagulation and flocculation through a series of jar tests. The entire quadratic model was developed using the analysis of variance [15]. SEM, XRD, and FTIR investigations were used to determine the surface morphology of the deposited sludge.

2. Materials and methods

2.1. Reagents

As a coagulant and flocculant, Louswolf, US Ltd.'s sodium bisulfate ($NaHSO_4$) solution and Aquachem, India's polyaluminum chloride (PAC) utilized, respectively. Sydney Solvent's hydrochloric acid (HCl) utilized to control the pH level of effluent during the treatment procedures [16]. HCl is used to alter pH. $NaHSO_4$ employed as a flocculant, and PAC is used as a coagulant. The concentrations of HCl 85%, PAC was between 30% and 40%, and $NaHSO_4$ was 0.20%. Table 1 describes the specifics of the utilized materials.

2.2. Standard solution preparation

By liquifying solid dye in distilled water, the brilliant green dye solution produced. 300 mg of the dye liquified per liter of distilled water to create the sample, which is like true commercial dye effluent [17]. The number of potassium chloride salts increased and tuned the conduction of the solutions.

2.3. Jar test

The standard method for optimizing the computation after adding coagulants and flocculants has been the jar test. The purpose of this preparation is to predict how synthetic coagulation–flocculation reduce the colloidal, suspended, and non-settable substance from the effluent. The variable amount bump in the coagulation–flocculation phase evaluated using the same standard [18]. It categorically decided to use 250 mL sample for each jar test due to the number of potential jar tests and the total effluent amount of 20 L available for all these tests. The resulting ideal pH and chemical dose then pragmatically applied to 650 and 950 mL of the remainder sample, with the same experimental results as those for 250 mL [19]. A workshop jar test made by Yatherm Scientific, India, with five parallel beakers was the equipment employed. Each beaker had a capacity of 250 mL for the brilliant green dye effluent. Hydrochloric acid (HCl) utilized to adjust the pH for coagulation, while sodium bisulfate solution [$NaHSO_4$] and polyaluminum chloride (PAC) used as coagulants in various mixes to promote flocculation. While flocculation required slow mixing at 50 rpm for 5 min, followed by 30 min of subsidence, coagulation required rapid mixing at 250 rpm for 5 min. Two sets of jar tests conducted in accordance with the conventional test procedures. Between 1.0 and 3.0 mL of coagulant and flocculant combined in the first series [20]. The pH ranges for coagulation and flocculation in the second sequence varied from 6 to 9 and 5 to 8, respectively. The supernatant's ultimate pH, COD, SS, colour, and turbidity were then controlled.

2.4. Analysis

Table 2 displays the procedures and tools used to measure pH, COD, SS, and turbidity. The Standard Methods were followed for all studies.

Table 1
Reagent characteristics

Chemicals	Formula	Physical form	Molecular weight (g/mol)
Hydrochloric acid	HCl	Liquid	36.458
Polyaluminum chloride	PAC	Powder	80.45
Sodium bisulfate	$NaHSO_4$	Liquid	120.06

Table 2
Analytical method and equipment's

Parameter	Method	Apparatus	Range
Turbidity	Nephelometry	Turbid metre (Sky Technology, India)	0.01–1,200 NTU
Suspended solids	Evaporation	Moisture analyser (Nordson, US)	1%–40%
pH	Electrometry	pH meter (Omega, India)	1–12
COD	Spectroscopy	Photometer (Hitech Lab, India)	10–10,000 mg/L

2.5. ANOVA analysis

An investigation technique in statistics called analysis of variance (ANOVA) separates methodical elements and random factors from an experiencing cumulative inconsistency originating from exclusive statistics established. It establishes the influence that an independent unknown has on the dependent variable in a regression analysis [21]. In this study, the relationship between the dependent and independent variables is determined using a one-way ANOVA. The ANOVA method has often been utilized to determine the significant outcome level of persuasion parameters on response. This strategy used in this study to stimulate each individual parameter's mean square competence, and the calculation results are analysed. The following equations are used in the ANOVA method to calculate the degree of freedom (DF), sum of squares (SS), mean of squares (MS), F values, and influence ratios of each parameter. Cross authentication, testing, and estimation are common methods for accomplishing this. The models for testing alone are used as the foundation for the calculation of testing [22]. In corporeal science, however, this is frequently not possible because there are typically insufficient examples. Then, a better technique is employed, which tries to do caricature forecast testing by repeatedly eliminating things from the data collection.

$$F = \frac{\text{MST}}{\text{MSE}}$$

where F = ANOVA coefficient; MST = mean sum of squares due to treatment; MSE = mean sum of squares due to error.

To enhance the erratic in the evolution of coagulation and flocculation, experimental data should be analysed using a second-order polynomial model. The analysis of alteration was also established by a design specialist.

2.6. Characterization

2.6.1. SEM analysis

The technique of SEM analysis resulted in the acquisition of floc pictures. The estimation of flocculation and aperture properties of surface area using geometrical data in two-dimensional photographs done using an image dispensation software package. This software's ability to control the edge to accurately mimic entity geometrical information eliminates the need for manual human verge alteration, which is one of its main advantages. This significantly reduces the quantile mistake generated by visual perception [23]. This type of software has been effectively employed by lab and other researchers to compute floc possessions in earlier works. In addition, to effectively avoid a potential loss of floc geometrical parameter data, flocs in more than 10 photos within 1 min used to determine floc size and fractal dimension at the consistent instant. This was in line with prior studies. Examining was done using scanning electron microscopes (SEM), specifically an APE-80 syrmaks P-480 SEM equipped with a 600 EDS spectrometer and an HDP-EDS detector, in order to confirm the deposited sludge during the flocculation process. Acerbating the samples and subjecting the saturated segments to a rasping procedure allowed for the execution of all extent on elegant segments [24]. To evaluate any compositional modification dependent on the complex array of various capabilities contained within the cohort of the analytical signals. The studies completed at a magnification of 600 to provide data that was at least passably illustrative. This resembles squares about 1 mm^2 in size. In both configurations, the analyses carried out by searching four areas for each taster.

2.6.2. XRD analysis

The elimination of BG dye in aqueous solution yielded a coagulant and flocculant base. Maximum predicted a dense resolution between cancrinite and hydroxycancrinite, whereas calcite and analyte are less important, are the primary components in BG as indicated by XRD. The mud's cation exchange capacity was only high, and its pH level was 8. Measurements of the overall concentration of the major and minor components in the coagulant made using a tube that stimulated X-ray fluorescence (XRF) [25]. To reduce background results and advance monochromaticity, quantity distributed utilizing an X-ray tube with a secondary board in orthogonal geometry. The operational parameters of the Topins X-ray apparatus model MSLH06 were 40 kV and 45 mA. 3,000 s were spent irradiating. A Si (Li) detector used to create the X-ray spectra, which were then analysed using the reiterative smallest quadrangular accurate computer code. As part of the quality control of the measurements, IFEA standard orientation material analyses were completed. A photograph taken inside the research coop as well as a representation schematic of the stream cell configuration at the Diamond Light Source [26]. Using a centrifugal micro-pump, a locally heated development brine is mixed within a bolted loop between the flow cell and a 2 L vessel. A coagulant sample with recorded electrochemical responses and diffraction patterns is housed in the stream cell. The arrangement's primary strength is that it supports in situ electrochemical dimension. The flowing brine makes it possible to achieve the deflection patterns. After the flow started

through the cell, the XRD measurements started 5–8 min after the pump was turned on since it took that long to finish the security checks and leave the experimental hutch.

2.6.3. FTIR analysis

Using a Spectrum Two-Perkin Elmer Model at room temperature, Fourier-transform infrared spectroscopy (FTIR) employed to observe the real clusters in molecular structures. The IR spectra used to monitor the actual assembly. The vibration of the band at 640 cm^{-1} is associated with (AlCl). Due to different surroundings, (Al–O's) vibration appeared in two distinct frequencies (Al–O) [27]. As a result, the peak at 1,874 cm^{-1} is like the NaCl bond expanding. Stretching and bending of the bands seen at 1,825 and 2,840 cm^{-1} are attributed to (OH). The vibration of the band at 3,252 cm^{-1} is (Al–OH). These allotted objects make up the coagulant stages. The characteristic peaks of the amide groups band in FTIR are useful for studying the structure of the deposited sludge since they offer a wealth of useful information [35]. Different temperature-treated coagulation–flocculation FTIR spectra were shown. The samples treated for 40 min at various temperatures (10°C, 30°C, 50°C, 70°C, and 90°C) [28]. FTIR spectra were obtained from discs containing coagulant-deposited sludge samples. The spectra were measured from 8,000 to 800 cm^{-1} using an infrared spectrophotometer at an 8 cm^{-1} per point data capture rate.

3. Result and discussion

3.1. Coagulation–flocculation process

The coagulation–flocculation procedure took five steps to complete. The pH of the effluent raised to 6.5 in the first step since 4.7–6.8 is the ideal pH range for polyaluminum chloride. Coagulant added in the second stage to destabilize the colloidal emulsion particle. In order to function best in the pH range of 4.7–9, pH was adjusted to 8.5 in the third phase using HCl [29]. The destabilized colloidal particles brought together to form larger flocs in the last step by the addition of a flocculant called sodium bisulfate. In the second series of trials, the pH values for coagulation and flocculation altered while the concentration of the coagulant and flocculant remained unchanged which is represented in Fig. 1. On the elimination of COD, suspended particles, colour, and turbidity, the effects of coagulant–flocculant concentration and pH were examined, respectively [30].

3.2. Removals of COD, suspended solids, colour and turbidity

3.2.1. pH study

At constant pH values of 4 for coagulation and 9 for flocculation, the effects of coagulant and flocculant dosages on the removals of COD, SS, and turbidity examined. pH is one of the stable measures that serves as a gauge for the acidic and basic states of water. Since most chemical processes in an aquatic environment are governed by changes in pH, this straightforward parameter is also very crucial [31]. Sample 1 (S1) had 0.5 mL of coagulant in the pH range of 4.5, Sample 2 (S2) had 1 mL of coagulant in the pH range of 5.2, Sample 3 (S3) had 1.5 mL of coagulant in the pH range of 6.3, Sample 4 (S4) had 2.0 mL of coagulant in the pH range of 7.6, and Sample 5 (S5) had 2.5 mL of coagulant in the pH range of 9, which all placed in Table 3 and Fig. 2.

3.3. COD study

The COD removal investigated during the coagulation and flocculation processes. During the coagulation research, the COD removal increased with the addition of more coagulant and flocculant doses until the maximum

Table 3
pH range of coagulant

Samples	Coagulant (mL)	pH ranges
S1	0.5	4.5
S2	1.0	5.2
S3	1.5	6.3
S4	2.0	7.6
S5	2.5	9.0

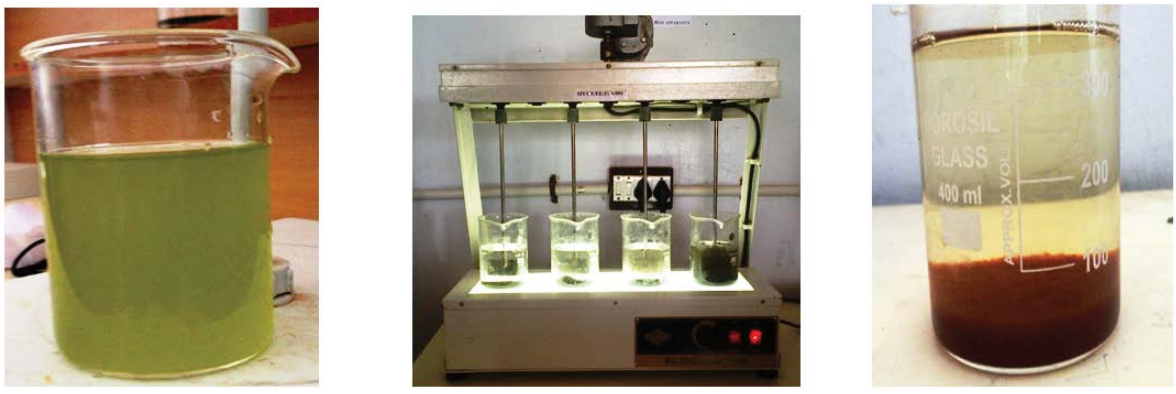

Fig. 1. (A) Concentrated Brilliant Green effluent, (B) Jar test experiment, and (C) deposited coagulant.

values attained. In the concentrated effluent, the COD between 6,500 mg/L. When the coagulant and flocculant doses 0.5 mL in the 250 mL S1 sample, the COD removal rate was around 15%, but it increased to 64% on the concentration of coagulant 1.0 mL, the COD concentration being 2,300 mg/L in S2, which is still insufficient for the needed standard [32]. The COD removal efficiency was 95.3% when the doses were increased to 1.5 mL (S3), 96.9% when they increased to 2.0 mL (S4), and 99.2% when they were increased to 2.5 mL (S5), as shown in Table 4 and Fig. 3, respectively. The COD removal efficiency was 96.9% when the doses increased to 200 mg/L (S4).

3.4. Turbidity study

The removal of turbidity during the coagulation and flocculation processes examined in Table 5. During the coagulation research, the removal of turbidity increased with the addition of more coagulant and flocculant dosages until the maximum values attained [33]. The concentrated wastewater had a turbidity range of 98NTU. It climbed to 63% on the concentration of coagulant of 1.0 mL in S2, which is still insufficient for the required level, when the doses of coagulant and flocculant 0.5 mL in 250 mL S1 sample. Increasing the doses to 1.5 mL (S3) allowed for the reduction of turbidity to reach 31 NTU. The S4 level's coagulant range was 2.0 mL with 18 NTU turbidity removal efficiency, while the S5 level's range was 2.5 mL with a 3 NTU removal, as shown in Fig. 4.

3.5. Suspended solids study

The removal of suspended particles during the coagulation and flocculation processes was studied (Table 6). During the coagulation research, the removal of suspended solids increased when the coagulant and flocculant doses raised until the maximum values attained [34]. The concentrated effluent included a range of suspended particles of 3,800 mg/L. The removal of suspended solids was around 76% in the 250 mL S1 sample when the coagulant and flocculant doses 0.5 and 1.0 mL, respectively. However, the concentration of suspended solids in the S2 sample was 2,030 mg/L, which is still insufficient for the required standard. When the doses increased to 1.5 mL (S3), 92.1% of the suspended solids removed in the range of 1,900 mg/L. At the next level, S4, the coagulant range was 2.0 mL, and the suspended solids removal efficiency was 95.3% with a concentration of 980 mg/L. At the final level, S5, the coagulant range was 2.5 mL, and 98.7% of the suspended solids were removed in the concentration of 520 mg/L.

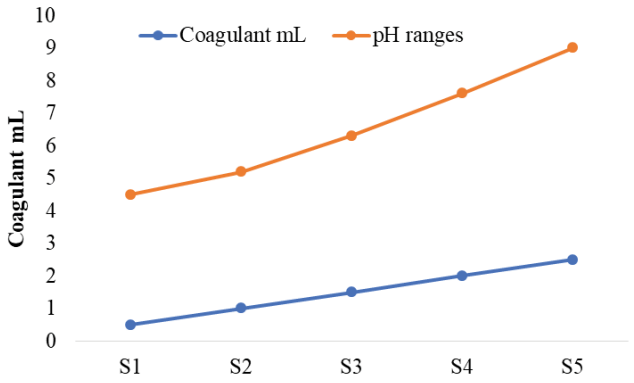

Fig. 2. Level pH in different coagulant concentration.

Table 4
COD removal

Samples	Coagulant (mL)	COD (mg/L)
S1	0.5	6500
S2	1.0	2300
S3	1.5	300
S4	2.0	200
S5	2.5	50

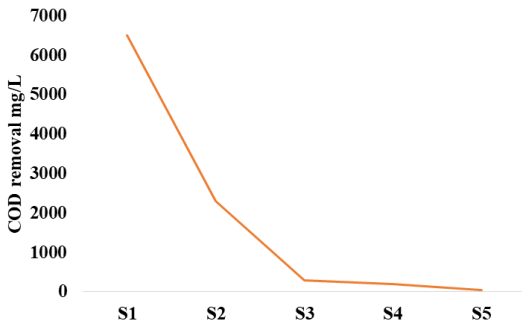

Fig. 3. COD removal efficiency in different dose.

Table 5
Turbidity removal

Samples	Coagulant (mL)	Turbidity (NTU)
S1	0.5	98
S2	1.0	63
S3	1.5	31
S4	2.0	18
S5	2.5	3

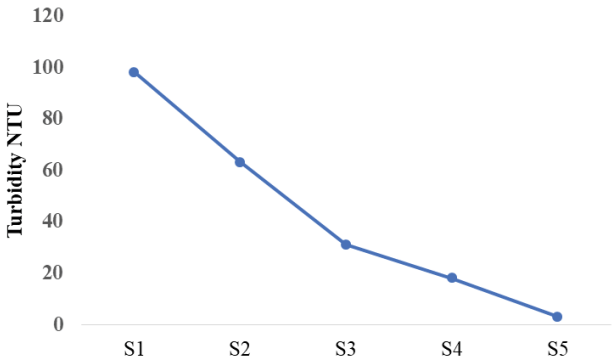

Fig. 4. Turbidity removal efficiency in different dose.

3.6. ANOVA variable analysis

The demand for justification with an attempt on forecast ability and consistency of the elements for interpretation arises as soon as the ANOVA model is obtained. The two most common techniques for doing this are annoyed authentication and forecast testing. A few samples are set aside for testing purposes exclusively during forecast testing. Incorporeal research, however, frequently finds this to be impossible because there are typically insufficient samples available [35]. Then, a better approach is to employ *F*-value and *p*-value, which imitates prediction testing by gradually removing objects from the data set. For instance, one might exclude entity 1 in the first round and model the remaining entities before testing the model on the initial object. This continues until every sample has been examined once. The progression is sometimes referred to as leave-one-out DF, or onefold SS, where one sample is omitted at a time. *F*-value is a hypothesis that says a model is significant if it has an *F*-value higher than *F*-critical. The models have an *F*-critical analysis since their *F*-values are 96.53 (Table 7). The *p*-value utilized to determine whether the *F*-value is large enough [36]. In other words, *p*-values < 0.003 show that the regression model is statistically significant. These models take into account both linear and quadratic effects as well as the two-way interactions between the variables under study. the representation of empirical correlation in mathematics. The correlation coefficient value acts as an evaluation of the model's adequacy based on the actual values of these elements created by the factors included.

3.7. Characterization

3.7.1. SEM results

Fig. 6 illustrates the surface morphologies of the coagulant at 800x and 2,000x magnifications following coagulation investigations that revealed holes of various sizes and shapes. The macropores and mesopores classifications are pore diameters that are unique to synthetic materials. Experimental results showed that the coagulant has a rough surface and is mostly constituted of sodium bisulfate and polyaluminum chloride, which supports its chemical makeup [37]. Through flocculation, interparticle bridging, or coagulation interactions, particles may be joined to these synthetic strands. A dense-net structure that is more conducive to particle coagulation and flocculation as a result of adsorption and bond generation among flocs as connected with branched structure also influenced by the morphology. Bulky clusters caused by element flocculation are shown in Fig. 6. Additionally, adsorption of particles on chemical surfaces has been linked to a reduction or filling of the number of holes on synthetic surfaces. SEM utilized to examine the surface morphology of the coagulant that had been deposition. Fig. 6 displays the SEM images of deposited coagulant. The coagulant's surface is ragged in contrast to its smooth counterpart [38]. The network structure created by the molecular bars of the component parts of coagulant promotes coagulation–flocculation and bridge performance of coagulant as a flocculent. The findings of the pore size measurement are shown in the histogram in Fig. 6. The histogram shows a hierarchy of pore types, from micropore to mesopore to fracture macropores. The lowest and highest average crystalline sizes are also shown below the histogram. [39]. The specified pore dimension areas for the synthetic metric image and pore dispersion are shown in Fig. 6. It exposed the coagulant–flocculant clustering in the surface atmosphere.

3.7.2. XRD analysis

The XRD spectrum showed potential coagulant chemical linkages. However, the goal of this experiment to use X-ray powder diffraction to identify the compounds or phases. The XRD of the coagulant–flocculant is shown in Fig. 7. Polyaluminum chloride and sodium bisulfate component rays were present in the surface morphology during the major phase of the spectrum [40]. This suggests that the coagulant should not simply be a mixture of the basic ingredients shown in Fig. 7 but rather a novel polycrystalline complex comprising polyaluminum chloride, sodium bisulfate, and other polymeric species [41]. Fig. 7 shows the XRD spectra of coagulant and flocculant samples with various synthetic molar ratios. The analysis's findings revealed that the grouping of these samples includes crystals of $NaHSO_4$, PAC, and HCl in addition to other crystals. For coagulant samples, a

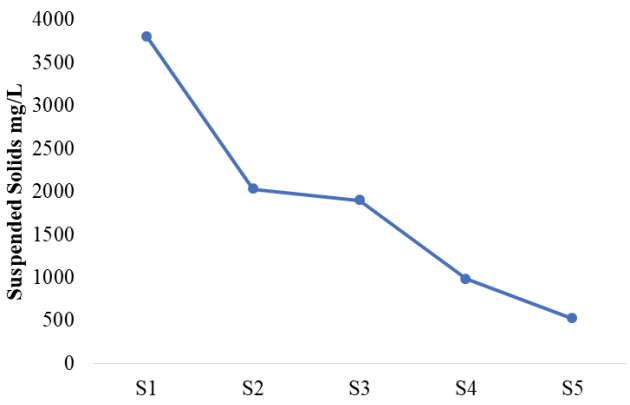

Fig. 5. Suspended solids removal efficiency in different dose.

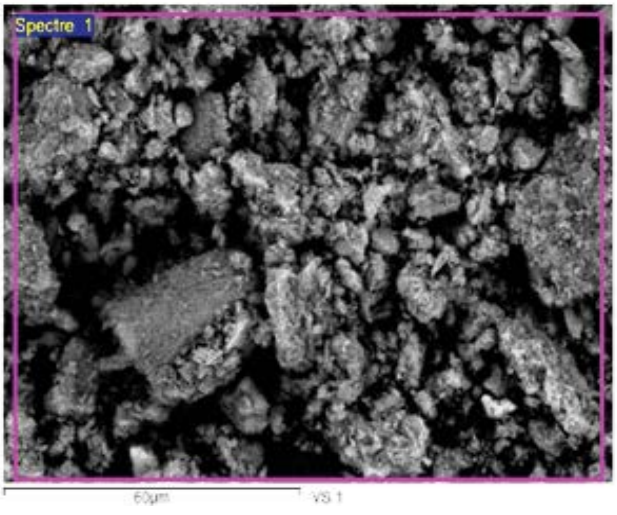

Fig. 6. SEM analysis of coagulant.

new peak at 20.0 was found, indicating that the composite coagulant had undergone some shaping. The XRD spectra also showed that $NaHSO_4$ had a larger concentration of the deflection peaks than PAC [42]. Additionally, the concentration of the deflection peak differed and the molar ratios were varied. Due to the cumulative nature of the coagulation–flocculation molar ratio, the intensity initially decreased, then increased, reaching its minimum value at a mole ratio of 10%. It stated that adding the right quantity of BG dye could result in improved scattering, larger ratios of the products' approximate structures, and decreased crystallinity [43]. It is also possible that the $NaHSO_4$-induced rise in the molecular weight of the BG resulted in shoddier chain section gesture, a restriction on fragment dispersion, and investiture to crystal, which helped attain subordinate crystallinity.

3.7.3. FTIR spectroscopy

Fig. 8's representation of the FT-IR spectrum for the coagulant reveals a broad absorption peak in the

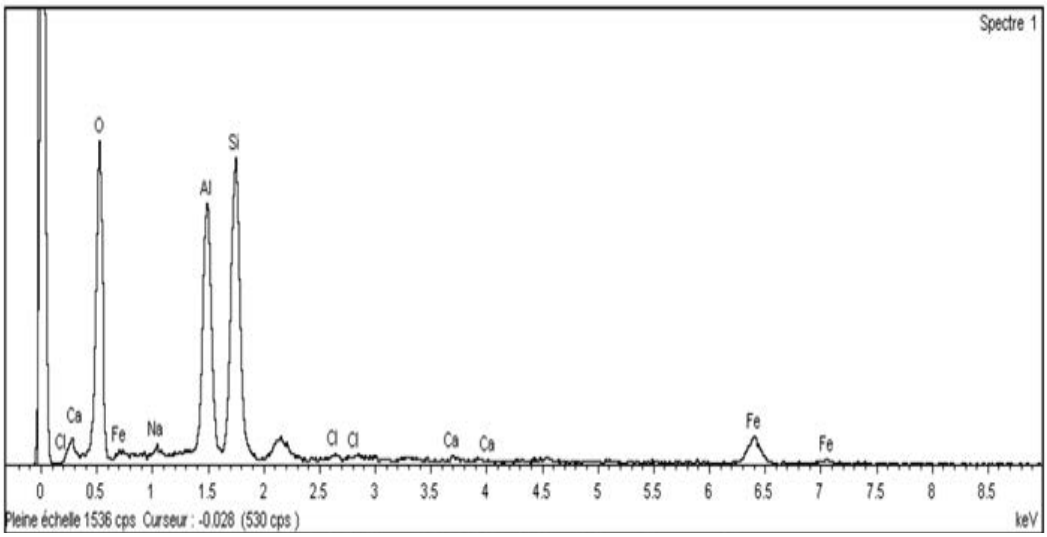

Fig. 7. XRD analysis of coagulant.

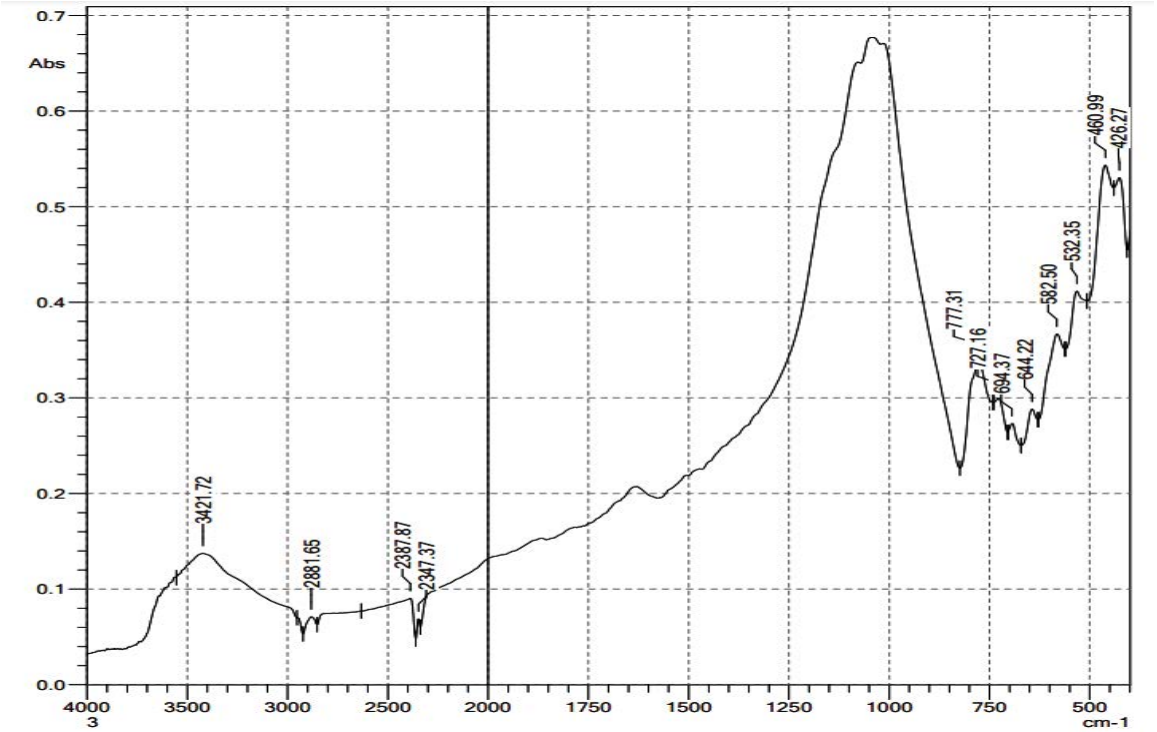

Fig. 8. FTIR analysis of coagulant.

Table 6
Suspended solid removal

Samples	Coagulant (mL)	Suspended solids (mg/L)
S1	0.5	3800
S2	1.0	2030
S3	1.5	1900
S4	2.0	980
S5	2.5	520

Table 7
ANOVA table for Brilliant Green removal efficiency

Source	DF	*F*-value	*p*-value
Model	3	96.53	0.000
Linear	2	147.86	0.000
pH	1	9.5	0.003
COD	2	471.3	0.000
Turbidity	1	43	0.012
SS	1	1,457.2	0.000

4,580–4,000 cm^{-1} range for both coagulants during flocculation, which is attributed to the stretching vibration of OH [44]. The medium peak in the region of 1,312–1,200 cm^{-1} is attributable to the bending vibration of the OH groups in water molecules, specifically the HOH angle distortion frequency, suggesting that the coagulant may contain structural and adsorbed water. For coagulant, the peaks at 1,145 and 1,120 cm^{-1} are responsible for the SO_4 stretching vibration. The peaks at 543 and 512 cm^{-1} for the coagulant are associated to the bending vibration of Fe–OH and Fe–O, respectively [45]. Fig. 8's FTIR spectrum of complex coagulants shows strong absorption peaks at 6,800–6,400 and 1,784 cm^{-1}, which are attributed to the expanding vibration of –OH and quivering of absorbed water. The proportional stretching vibrations of Na–OH–Na and Na–O, respectively, detected as the peaks at 743 and 812 cm^{-1}, respectively. This suggested that the coagulant that had been prepared was a coagulant sympathetic to those created by the OH bridges. On the peak shapes of PAC and $NaHSO_4$, no notable changes were found [46]. The establishment of the new Na–OH connection between the PAC may be blamed for the appearance of a new crowning at approximately 1,264 cm^{-1}. As opposed to a straightforward combination of the raw components, $NaHSO_4$-PAC was more resistant to defining new chemical species. The molecular weight of the coagulant and the accumulating charge of a single particle increase as Na^{3+} strength builds up [47]. These changes may be beneficial for bridging and adsorption, charge neutralization, and co-precipitation netting. While the peak morphologies of the PAC samples almost identical, $NaHSO_4$-PAC had a higher concentration of the absorption peak at 1,452 and 1,647 cm^{-1}. This proved that Ce^{3+} accumulation order could stimulate Ce–OH–Fe growth [48]. The order of PAC and $NaHSO_4$ build-up harmful for producing the compound coagulant. The blueshift of samples with the maximum absorption at around 821 cm^{-1} was pragmatically related to the PAC sample. It was primarily caused by $NaHSO_4$'s stronger organizational capabilities than PAC, which strengthened the link between Na–O and Na–O–Na. Although this mountain transformed for its state [49]. It might be attributed to the fact that the increase in Ho encouraged the substitution of Na and thus sparked the emergence of some Na–OH–Na. The blueshift was therefore translated as weak.

4. Conclusion

Brilliant green dye treated using a synthetic coagulation–flocculation technique that was investigated. Coagulation–flocculation therapy proven to be a quick and effective way to get rid of BG dye. The original pH of the solution, any potential change in turbidity, SS, color, and COD all affect how effectively BG is excluded. Turbidity removal ranged from 40% to 98%, whereas SS and COD removal ranged from 15% to 99.2% and 20% to 97.3%, respectively. The jar tests reveal, however, that the treatment advancement very slight in relation to the pH levels and the doses of coagulants and flocculants utilized for effluent treatment. The key parameters (COD 6,500 mg/L, SS 3,800 mg/L, and turbidity 98 NTU) successfully brought to their target values using the coagulant and flocculant doses of 2.5 mL, respectively. The results of the jar test further supported by a successful pilot-scale experiment to remove BG dye using sodium bisulfate ($NaHSO_4$) and polyaluminum chloride (PAC) as coagulants and flocculants, respectively. The analysis of FTIR, SEM, and XRD revealed that the reactions between PAC and $NaHSO_4$ not simply physical mixtures but rather resulted in the formation of the new bond Na–OH–Na. After the build-up of Na^{3+}, the coagulant's molecular weight and the accretion charge of the single element both increased. The *F*-critical analysis for the ANOVA models is performed since their *F*-values are 96.53. The *F*-large value's sufficiency was controlled by the *p*-value. The findings of the regression model are statistically significant when the *p*-value is less than 0.003. The decolorization rate of straight green when treated with $NaHSO_4$-PAC may reach 99%. Under the same conditions, the decolorization rate of direct green wastewater was higher than that of directly debauched burgundy dye wastewater. It has been established that the chemical coagulation and flocculation method is a workable option for the treatment of BG dye in aqueous solution.

Conflict of interest

The authors declare no conflict of interest.

Acknowledgment

The authors extend their appreciation to the Researchers Supporting Project number (RSP2023R381), King Saud University, Riyadh, Saudi Arabia.

References

[1] B. Padmaja, S. Dhanapandian, S. Suthakaran, K. Ashokkumar, N. Krishnakumar, Hydrothermally developed SnO_2 nanoparticles and its photocatalytic degradation of Alizarin red S, Brilliant green and Methyl orange dyes and electrochemical

performances, Inorg. Chem. Commun., 149 (2023) 110363, doi: 10.1016/J.INOCHE.2022.110363.
[2] A. Ansari, M.M. Khoram, D. Nematollahi, G. Azarian, E. Niknam, A. Khalaj, A comprehensive study on opium pharmaceutical wastewater treatment in laboratory and semi-industrial scales, J. Water Process Eng., 44 (2021) 102353, doi: 10.1016/J.JWPE.2021.102353.
[3] A. Terracciano, J. Ge, X. Meng, A comprehensive study of treatment of arsenic in water combining oxidation, coagulation, and filtration, J. Environ. Sci., 36 (2015) 178–180.
[4] M. Ghaedi, A. Ansari, F. Bahari, A.M. Ghaedi, A. Vafaei, A hybrid artificial neural network and particle swarm optimization for prediction of removal of hazardous dye brilliant green from aqueous solution using zinc sulfide nanoparticle loaded on activated carbon, Spectrochim. Acta, Part A, 137 (2015) 1004–1015.
[5] A.M. Atta, H.A. Al-Lohedan, Z.A. ALOthman, A.A. Abdel-Khalek, A.M. Tawfeek, Characterization of reactive amphiphilic montmorillonite nanogels and its application for removal of toxic cationic dye and heavy metals water pollutants, J. Ind. Eng. Chem., 31 (2015) 374–384.
[6] A.M. Ghaedi, M. Ghaedi, A.R. Pouranfard, A. Ansari, Z. Avazzadeh, A. Vafaei, I. Tyagi, S. Agarwal, V.K. Gupta, Adsorption of Triamterene on multi-walled and single-walled carbon nanotubes: artificial neural network modeling and genetic algorithm optimization, J. Mol. Liq., 216 (2016) 654–665.
[7] S. Chen, Z. Yuan, D. Hanigan, P. Westerhoff, H. Zhao, J. Ni, Coagulation behaviors of new covalently bound hybrid coagulants (CBHyC) in surface water treatment, Sep. Purif. Technol., 192 (2018) 322–328.
[8] M. Ghaedi, A. Ansari, R. Sahraei, ZnS:Cu nanoparticles loaded on activated carbon as novel adsorbent for kinetic, thermodynamic and isotherm studies of Reactive orange 12 and Direct yellow 12 adsorption, Spectrochim. Acta, Part A, 114 (2013) 687–694.
[9] G. Kheraldeen Kara, M. Rabbani, Experimental study of methylene blue adsorption from aqueous solutions onto Fe_3O_4/NiO nano mixed oxides prepared by ultrasonic assisted co-precipitation, J. Nanostruct., 9 (2019) 287–300.
[10] W. Song, Y. Xie, Q. Chen, W. Wang, X. Li, Investigation of polyaluminum chloride (PACl) coagulation to remove cyanobacteria from maintenance to decay stage: performance and mechanism, J. Environ. Chem. Eng., 10 (2022) 108395, doi: 10.1016/J.JECE.2022.108395.
[11] W. Tang, H. Li, L. Fei, B. Wei, T. Zhou, H. Zhang, The removal of microplastics from water by coagulation: a comprehensive review, Sci. Total Environ., 851 (2022) 158224, doi: 10.1016/J.SCITOTENV.2022.158224.
[12] T. Bertrand, M.A. Kahre, R. Urata, A. Määttänen, F. Montmessin, R.J. Wilson, M.J. Wolff, Impact of the coagulation of dust particles on Mars during the 2018 global dust storm, Icarus, 388 (2022) 115239, doi: 10.1016/J.ICARUS.2022.115239.
[13] X. Wang, H. Liu, C. Shan, W. Zhang, B. Pan, A novel combined process for efficient removal of Se(VI) from sulfate-rich water: sulfite/UV/Fe(III) coagulation, Chemosphere, 211 (2018) 867–874.
[14] D. Im, N. Nakada, Y. Fukuma, Y. Kato, H. Tanaka, Performance of combined ozonation, coagulation and ceramic membrane process for water reclamation: effects and mechanism of ozonation on virus coagulation, Sep. Purif. Technol., 192 (2018) 429–434.
[15] J.F. Zhang, Q.H. Zhang, J.P.Y. Maa, Coagulation processes of kaolinite and montmorillonite in calm, saline water, Estuarine Coastal Shelf Sci., 202 (2018) 18–29.
[16] W.L. Ang, A.W. Mohammad, A. Benamor, N. Hilal, Hybrid coagulation–NF membrane processes for brackish water treatment: effect of pH and salt/calcium concentration, Desalination, 390 (2016) 25–32.
[17] Q. Ding, H. Yamamura, N. Murata, N. Aoki, H. Yonekawa, A. Hafuka, Y. Watanabe, Characteristics of meso-particles formed in coagulation process causing irreversible membrane fouling in the coagulation-microfiltration water treatment, Water Res., 101 (2016) 127–136.
[18] Y. Li, G.D. Bland, W. Yan, Enhanced arsenite removal through surface-catalyzed oxidative coagulation treatment, Chemosphere, 150 (2016) 650–658.
[19] N. Shirasaki, T. Matsushita, Y. Matsui, T. Marubayashi, K. Murai, Investigation of enteric adenovirus and poliovirus removal by coagulation processes and suitability of bacteriophages MS2 and ϕX174 as surrogates for those viruses, Sci. Total Environ., 563–564 (2016) 29–39.
[20] C. Thamaraiselvi, A.A. Jenifer, M. Vasanthy, Coagulation Performance Evaluation of Natural and Synthetic Coagulants for the Treatment of Sugar Wash, Wastewater Recycl. Manag. 7th IconSWM—ISWMAW 2017, Vol. 3, 2019, pp. 53–64. https://doi.org/10.1007/978-981-13-2619-6_5/COVER
[21] H. Harfouchi, D. Hank, A. Hellal, Response surface methodology for the elimination of humic substances from water by coagulation using powdered Saddled Sea bream scale as coagulant-aid, Process Saf. Environ. Prot., 99 (2016) 216–226.
[22] B.A. Nordmark, T.M. Przybycien, R.D. Tilton, Comparative coagulation performance study of Moringa oleifera cationic protein fractions with varying water hardness, J. Environ. Chem. Eng., 4 (2016) 4690–4698.
[23] D. Jang, J. Lee, A. Jang, Impact of pre-coagulation on the ceramic membrane process during oil-water emulsion separation: fouling behavior and mechanism, Chemosphere, 313 (2023) 137596, doi: 10.1016/J.CHEMOSPHERE.2022.137596.
[24] X. Hu, P. Hu, H. Yang, Influences of charge properties and hydrophobicity on the coagulation of inorganic and organic matters from water associated with starch-based coagulants, Chemosphere, 298 (2022) 134346, doi: 10.1016/J.CHEMOSPHERE.2022.134346.
[25] J. Qi, H. Lan, R. Liu, H. Liu, J. Qu, Fe(II)-regulated moderate pre-oxidation of *Microcystis aeruginosa* and formation of size-controlled algae flocs for efficient flotation of algae cell and organic matter, Water Res., 137 (2018) 57–63.
[26] H. Li, H. Pei, H. Xu, Y. Jin, J. Sun, Behavior of *Cylindrospermopsis raciborskii* during coagulation and sludge storage – higher potential risk of toxin release than *Microcystis aeruginosa*?, J. Hazard. Mater., 347 (2018) 307–316.
[27] H.C. Kim, In-line coagulation with quaternary amine polymer prior to microfiltration of humic-rich water, J. Colloid Interface Sci., 459 (2015) 151–159.
[28] X. Li, Y. Zhang, X. Zhao, N. Gao, T. Fu, The characteristics of sludge from enhanced coagulation processes using PAC/PDMDAAC composite coagulants in treatment of micro-polluted raw water, Sep. Purif. Technol., 147 (2015) 125–131.
[29] C. Hu, Q. Chen, H. Liu, J. Qu, Coagulation of methylated arsenic from drinking water: influence of methyl substitution, J. Hazard. Mater., 293 (2015) 97–104.
[30] J. Song, J. Wang, D. Wang, Changes in the structural characteristics of EfOM during coagulation by aluminum chloride and the effect on the formation of disinfection byproducts, J. Environ. Manage., 326 (2023) 116850, doi: 10.1016/J.JENVMAN.2022.116850.
[31] B. Wang, Y. Nie, Z. Kang, X. Liu, Effects of coagulating conditions on the crystallinity, orientation and mechanical properties of regenerated cellulose fibers, Int. J. Biol. Macromol., 225 (2023) 1374–1383.
[32] S. Van Haute, M. Uyttendaele, I. Sampers, Coagulation of turbidity and organic matter from leafy-vegetable wash-water using chitosan to improve water disinfectant stability, LWT - Food Sci. Technol., 64 (2015) 337–343.
[33] J.Q. Jiang, The role of coagulation in water treatment, Curr. Opin. Chem. Eng., 8 (2015) 36–44.
[34] B. Deng, H. Luo, Z. Jiang, Z.J. Jiang, M. Liu, Co-polymerization of polysilicic-zirconium with enhanced coagulation properties for water purification, Sep. Purif. Technol., 200 (2018) 59–67.
[35] J. Zulewska, J. Kowalik, A. Lobacz, B. Dec, Short communication: calcium partitioning during microfiltration of milk and its influence on rennet coagulation time, J. Dairy Sci., 101 (2018) 10860–10865.
[36] B.A. Nordmark, T.M. Przybycien, R.D. Tilton, Effect of humic acids on the kaolin coagulation performance of *Moringa oleifera* proteins, J. Environ. Chem. Eng., 6 (2018) 4564–4572.

[37] N. Kataria, V.K. Garg, Application of EDTA modified Fe_3O_4/ sawdust carbon nanocomposites to ameliorate methylene blue and brilliant green dye laden water, Environ. Res., 172 (2019) 43–54.
[38] Q. Yang, J. Li, X. Wang, H. Peng, H. Xiong, L. Chen, Dual-emission color-controllable nanoparticle based molecular imprinting ratiometric fluorescence sensor for the visual detection of Brilliant Blue, Sens. Actuators, B, 284 (2019) 428–436.
[39] K. Mengal, G. Kor, A. Kouba, P. Kozák, H. Niksirat, Hemocyte coagulation and phagocytic behavior in early stages of injury in crayfish (Arthropoda: Decapoda) affect their morphology, Dev. Comp. Immunol., 141 (2023) 104618, doi: 10.1016/J.DCI.2022.104618.
[40] A.G. Raju, B.D. Rao, G. Himabindu, S.M. Botsa, Fabrication of a heterostructure composite with CuO and FeS_2 as efficient photocatalyst for decolourisation of brilliant green, J. Mater. Res. Technol., 17 (2022) 2648–2656.
[41] A. Aichour, H. Zaghouane-Boudiaf, Highly brilliant green removal from wastewater by mesoporous adsorbents: kinetics, thermodynamics and equilibrium isotherm studies, Microchem. J., 146 (2019) 1255–1262.
[42] H. Zeng, C. Liu, H. Xu, R. Hao, J. Zhang, D. Li, Preparation of Fe_3O_4@C with water treatment residuals and its potential in the magnetic coagulation process, J. Cleaner Prod., 362 (2022) 132327, doi: 10.1016/J.JCLEPRO.2022.132327.
[43] W. Yu, L.C. Campos, N. Graham, Application of pulsed UV-irradiation and pre-coagulation to control ultrafiltration membrane fouling in the treatment of micro-polluted surface water, Water Res., 107 (2016) 83–92.
[44] T. Asami, H. Katayama, J.R. Torrey, C. Visvanathan, H. Furumai, Evaluation of virus removal efficiency of coagulation-sedimentation and rapid sand filtration processes in a drinking water treatment plant in Bangkok, Thailand, Water Res., 101 (2016) 84–94.
[45] T.B. Mbuyazi, P.A. Ajibade, Structural studies and photocatalytic degradation of brilliant green by dodecylamine capped tin sulphide nanocrystals, Results Mater., 16 (2022) 100328, doi: 10.1016/J.RINMA.2022.100328.
[46] R.G. El-Sharkawy, Anchoring of green synthesized silver nanoparticles onto various surfaces for enhanced heterogeneous removal of brilliant green dye from aqueous solutions with error analysis study, Colloids Surf., A, 583 (2019) 123871, doi: 10.1016/J.COLSURFA.2019.123871.
[47] J.C. Cardenas, C.M. Rein-Smith, F.C. Church, Overview of blood coagulation and the pathophysiology of blood coagulation disorders, Encycl. Cell Biol., 1 (2016) 714–722.
[48] O. Bello, Y. Hamam, K. Djouani, Multiple model predictive control based on fuzzy switching scheme of a coagulation chemical dosing unit for water treatment plants, IFAC-PapersOnLine, 48 (2015) 180–185.
[49] J. Dasgupta, D. Mondal, S. Chakraborty, J. Sikder, S. Curcio, H.A. Arafat, Nanofiltration based water reclamation from tannery effluent following coagulation pretreatment, Ecotoxicol. Environ. Saf., 121 (2015) 22–30.